Permeability of solid foam: Effect of pore connections

Article *in* PHYSICAL REVIEW E · May 2018

DOI: 10.1103/PhysRevE.97.053111

7 authors, including:

Vincent Langlois
University of Paris-Est
35 PUBLICATIONS **217** CITATIONS
SEE PROFILE

Van Hai Trinh
Le Quy Don Technical University
16 PUBLICATIONS **92** CITATIONS
SEE PROFILE

Camille Perrot
Université Gustave Eiffel
79 PUBLICATIONS **1,024** CITATIONS
SEE PROFILE

Xavier Chateau
French National Centre for Scientific Research
93 PUBLICATIONS **3,019** CITATIONS
SEE PROFILE

Permeability of solid foam: Effect of pore connections

V. Langlois,[1,*] V. H. Trinh,[2,†] C. Lusso,[3,‡] C. Perrot,[2,§] X. Chateau,[3,‖] Y. Khidas,[4,¶] and O. Pitois[5,**]

[1]*Université Paris-Est, Laboratoire Géomatériaux et Environnement (EA 4508), UPEM, F-77454, Marne-la-Vallée, France*

[2]*Université Paris-Est, Laboratoire Modélisation et Simulation Multi Échelle, MSME UMR 8208 CNRS, Marne-la-Vallée 77454, France*

[3]*Université Paris-Est, Laboratoire Navier, UMR 8205 CNRS, École des Ponts ParisTech, IFSTTAR Marne-la-Vallée, France*

[4]*Université Paris-Est, Laboratoire Navier, UMR 8205 CNRS, École des Ponts ParisTech, IFSTTAR, 5 Bd Descartes, 77454 Marne-la-Vallée, France*

[5]*Université Paris-Est, Laboratoire Navier, UMR 8205 CNRS, École des Ponts ParisTech, IFSTTAR cité Descartes, 2 allée Kepler, 77420 Champs-sur-Marne, France*

(Received 21 December 2017; revised manuscript received 30 April 2018; published 31 May 2018)

In this paper, we study how the permeability of solid foam is modified by the presence of membranes that close partially or totally the cell windows connecting neighboring pores. The finite element method (FEM) simulations computing the Stokes problem are performed at both pore and macroscopic scales. For foam with fully interconnected pores, we obtain a robust power-law relationship between permeability and aperture size. This result is due to the local pressure drop mechanism through the aperture as described by Sampson for fluid flow through a circular orifice in a thin plate. Based on this local law, pore-network simulation of simple flow is used and is shown to reproduce FEM results. Then this low computational cost method is used to study in detail the effect of an open window fraction on the percolation properties of the foam pore space. The results clarify the effect of membranes on foam permeability. Finally, Kirkpatrick's model is adapted to provide analytical expressions that allow for our simulation results to be successfully reproduced.

DOI: 10.1103/PhysRevE.97.053111

I. INTRODUCTION

Foam is a dispersion of gas in liquid or solid matrix. Its structure is made of membranes (also called films for liquid foams), ligaments or Plateau's borders (junction of three membranes), and vertices or nodes (junction of four ligaments). Whereas closed membranes are necessary to ensure the mechanical stability of liquid foam [1], membranes can be open or totally absent in solid foam, allowing for the foam cells (pores) to be connected through windows. It is remarkable that such a small volume contained in the window areas can have such drastic effects for several properties of foams. This is the case for fluid permeability of solid foam, where open windows contribute to transport the fluid through the material, whereas closed windows stop it. Therefore, the fraction of closed windows is crucial for several applications, such as filtering. As viscous dissipation is the most dissipative mechanism in sound propagation through porous materials, permeability (or flow resistivity) is a key parameter in this issue [2,3], making acoustical properties of foams very sensitive to both the open window fraction and the aperture size of windows. Different works have focused on the effects of foam geometry on permeability: fraction of closed windows [4], aperture of windows [5], and solid volume fraction and ligament shapes [6,7]. Authors have proposed empirical relations between permeability and several structural parameters of foam (solid volume fraction, window aperture rate, etc.), but a global physical model would be suitable in order to design foams with the required permeability. Note also that, beyond a critical value of open window fraction (called the percolation threshold), the percolation phenomenon is expected to arise in foams, i.e., the size of the largest cluster of interconnected cells is equal to the sample thickness, H_{sp}, leading to an open pore space [8]. This phenomenon has not been studied so far in the case of foams, although it has been proved to have a great influence on permeability of porous media. For example, the classical Kozeny-Carman equation has to be modified by considering the difference between the porosity and the critical porosity leading to percolation [9]. Tackling the percolation issue for the permeability of porous media requires numerical simulations to use large samples involving a few thousand pores [10]. For the flow simulation at the pore scale or at the scale of a few pores, the finite element, finite volume, boundary element, and lattice Boltzmann methods have been often applied [3,11–13]. However, as the size of samples increases, the computational costs for those methods become prohibitive, so that multiscale approaches are preferable [14–19]. Such methods involve determining the flow behavior at the local scale (i.e., a throat between two linked pores) by numerical simulations or analytical solutions (e.g., Hagen-Poiseuille equation); then pore-network simulations are performed to determine the permeability at the macroscopic scale [20].

In this paper, we use a multiscale approach to study the permeability of solid foam with various windows configurations. The effect of aperture size on local permeability

*vincent.langlois@u-pem.fr

†van-hai.trinh@u-pem.fr; Also at Le Quy Don Technical University, Hanoi, Vietnam.

‡christelle.lusso@onera.fr

§camille.perrot@u-pem.fr

‖xavier.chateau@enpc.fr

¶yacine.khidas@u-pem.fr

**olivier.pitois@ifsttar.fr

of fully open-cell foam (i.e., containing no closed window) is studied by using FEM simulations on periodic unit cells (PUCs) with the Kelvin partition of space. The effect of closed windows is studied through FEM simulations on larger samples (containing 256 pores). Then mesoscopic effects induced by the structure of the pore network are studied by pore-network simulations on large (containing at least 43 900 pores) networks of interconnected pores interacting via local permeabilities. Finally, a model of effective permeability, based on a calculation of the mean local permeability as in Kirkpatrick [14], is used to provide a physical description of the membrane-induced percolation effect in foam and the effect of combining several local permeabilities.

II. NUMERICAL SIMULATIONS OF FOAM PERMEABILITY

A. FEM Simulations of fluid flow

1. At the pore scale

As shown in Fig. 1, a periodic unit cell of size D_b is used to represent the pore structure in foam samples [21]. The number of pores, N_p, contained within the unit cell is equal to 2. The cell is based on the Kelvin paving and is a 14-sided polyhedron (eight hexagons and six squares) corresponding to windows shared with the $N_v = 14$ neighbors. The cell skeleton is made of idealized ligaments having length $L = D_b/(2\sqrt{2})$ and an equilateral triangular cross section of edge side $r = 0.58 D_b(1-\phi)^{0.521}$, where ϕ is the gas volume fraction [1]. As we are interested here in the effect of partial closure of the cell windows by membranes, we partially close the windows by adding holed membranes characterized with distinct circular aperture sizes. Two kinds of simulations were performed: (1) identical aperture size for all windows [Fig. 1(b)] and (2) identical rate of aperture $\delta_{\text{ow}} = t_o/t_w$ [Fig. 1(c)] where t_w and t_o are, respectively, the full window size and the size of the aperture

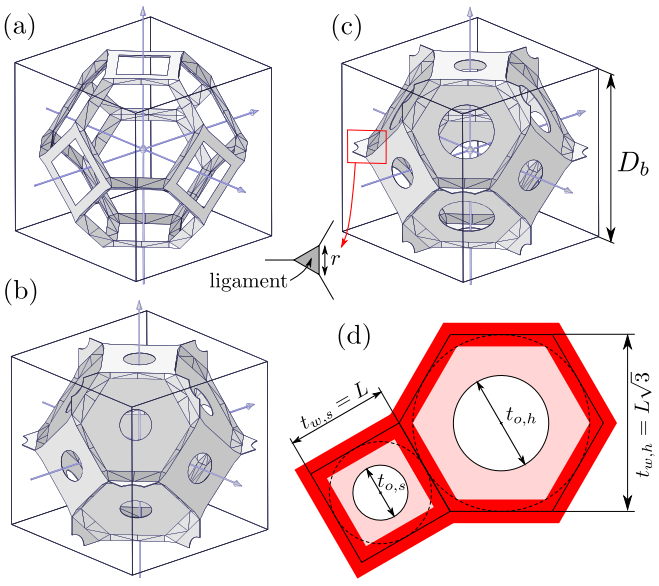

FIG. 1. PUC with fully open windows (a), with partially closed windows characterized by the same aperture size (b), identical aperture rate (c), definitions of the aperture size t_o, and the full window size t_w (d).

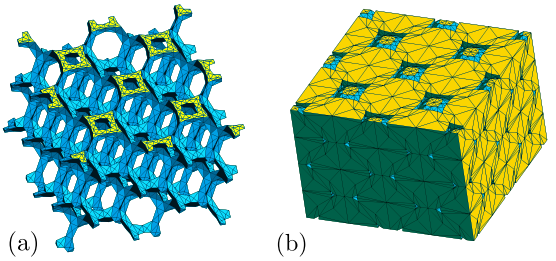

FIG. 2. FEM macroscale samples: skeleton mesh (a) and pore-space mesh (b). For sake of visibility, a mesh of size $2\sqrt{2} \times 2\sqrt{2} \times 2$ (D_b units) is depicted.

as defined in Fig. 1(d). Note that, in the reference configuration [Fig. 1(a)], the 14 cell windows are fully open (i.e., contain no membrane). The static viscous permeability K is computed from the solution of the Stokes problem [8] for different porosities. The boundary value problem is solved by using the finite element method and the commercial software COMSOL Multiphysics. The permeability calculation error, determined by convergence tests, is inferior to 6%. To achieve this accuracy, the meshes contain at least 250 000 tetrahedral elements.

2. At the macroscopic scale

In order to study the flow properties on a larger scale, we have performed numerical simulations for the flow of a Newtonian fluid through a periodic network of Kelvin cells having a size $L \times L \times H_{\text{sp}} = 4\sqrt{2} \times 4\sqrt{2} \times 4$ in D_b units (i.e., $N_p = 256$ pores), and a porosity ϕ equal to 0.9. Figure 2 shows an open cell foam sample made of 32 pores (i.e., all the windows between adjacent cells are open). The macroscopic intrinsic permeability is computed from the averaging of the solution of the Stokes problem set on the foam sample. In this study, the cell windows are either closed or open with random spatial distribution over the foam sample. The fraction of open windows is $x_{\text{ow}} = N_{\text{ow}}/(N_p \times N_v/2)$, where N_{ow} is the total number of open windows. For each value x_{ow}, the macroscopic intrinsic permeability is the average of numerical simulations for six different samples obtained from six random draws of closed window positions. The resolution of the boundary value problem is achieved through the Finite Element Method using FreeFem++ software [22]. The typical discrete problem contains 1 400 000 tetrahedra and 8 000 000 degrees of freedom and is solved using a Message Passing Interface on four processors. We compared the permeability computed with the finest mesh (1 400 000 tetrahedra) to the permeability computed using a coarser one (700 000 tetrahedra). As the difference is less than 3%, which is small compared to the window closure induced permeability variations, we concluded that the meshes we use are fine enough for accurate results.

B. Pore-network simulations

Effects of pore network features on permeability are studied on several lattices having different numbers of neighbor pores N_v (Fig. 3). Concerning foam, the cases $N_v = 14$ and $N_v = 8$ are of specific interest: $N_v = 14$ corresponds to Kelvin's structure, which is very relevant to describe foam's structure [1], and $N_v = 8$ corresponds to BCC structure, or to Kelvin's structure

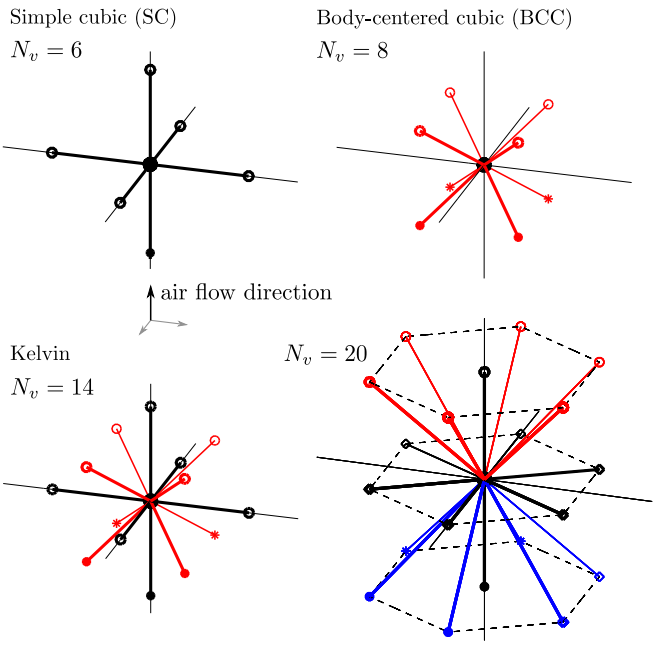

FIG. 3. Network structures used in pore-network simulations.

with the smallest windows (square windows) being closed as expected for a small fraction of gas ϕ. For $N_v = 14$ and $N_v = 8$, the samples have a size $L^2 \times H_{\rm sp} = 28^3$ (D_b units) and contain 43 904 pores. For $N_v = 6$ and $N_v = 20$, the samples contain at least 46 000 pores. Boundary effects are avoided by resorting to periodic conditions imposed in the directions perpendicular to the macroscopic flow. In this simple model, we consider, for each pore, a unique value of pressure without calculating the fluctuations of pressure and fluid velocity inside the pore. At the local scale, the flow rate $q_{j\to i}$ from pore j to pore i is governed by the differential pressure between the pores $\Delta P_{ij} = P_j - P_i$, $q_{j\to i} = \frac{D_b}{\mu} k_{ij} \Delta P_{ij}$, where the coefficient k_{ij} is the local permeability between the pores i and j, and μ is the dynamic viscosity of the fluid.

At steady state and by considering incompressible fluid, the volume of fluid inside pore i is constant and the sum of flow rates coming from neighbor pores is equal to zero, leading to $\sum_{j=1}^{N_v} k_{ij}(P_j - P_i) = 0$. To generate a flow through the sample, a pressure difference is imposed between top and bottom faces of the sample ($P_{\rm top} = \Delta P_{\rm sp}$, $P_{\rm bot} = 0$). By considering these boundary conditions, this previous equation can take a matrix form:

$$\bar{K}[P_i] = [S_i], \tag{1}$$

where $[P_i]$ is a vector containing the pressure of inner pores (pores located on the top and bottom faces are excluded); $\bar{K}$ is the matrix defined from local permeabilities ($-\sum k_{ij}$ along the diagonal and k_{ij} elsewhere); and $[S_i]$ is a vector containing zeros except for inner pores having top pores as neighbors where $S_i = -\sum_{j_{\rm top}} k_{ij_{\rm top}} \Delta P_{\rm sp}$.

As soon as the pore network links top to bottom and by considering only the interconnected pores, $\bar{K}$ can be inverted and the fluid pressure in each pore can be calculated from Eq. (1). Alternatively, in the case of memory limitations during computer calculations, fluid pressure can be calculated in an iterative way as in Ref. [14]. In any way, from fluid pressures, the macroscopic flow Q and the macropermeability K can be calculated as

$$Q = \sum_{i_{\rm bot}} \sum_{j_v} q_{j_v \to i_{\rm bot}} = \frac{D_b}{\mu} \sum_{i_{\rm bot}, j_{vi}} k_{i_{\rm bot} j_{vi}} \Delta P_{i_{\rm bot}, j_{vi}}, \tag{2a}$$

$$K = \mu Q H_{\rm sp} / L^2 \Delta P_{\rm sp}. \tag{2b}$$

Different materials having different kinds of local permeability distribution were studied: two local permeabilities (binary mixture), a local permeability mixed with zero permeability (i.e., closed window), and two local permeabilities mixed with closed windows. For each kind of local permeability distribution, calculations were repeated 100 times on different random draws in order to calculate an average. For each random draw, local permeabilities were randomly distributed over the network.

To reduce errors induced by size effects in the calculation of percolation threshold and open porosity (defined as the volume fraction of pores occupied by percolating fluid) [10], additional numerical simulations were performed on large samples such as $N_p \sim 10^6$ pores.

III. RESULTS AND DISCUSSION

A. Effect of the aperture size

FEM simulations on PUCs at the pore scale for various aperture sizes reveal a power-law relationship between permeability and aperture size [Fig. 4(a)]. Similarly the numerical results for the dimensionless permeability of porous materials with same aperture rate are well fitted by a power law when plotted in a ($\delta_{\rm ow}$, K/D_b^2) diagram [Fig. 4(b)]. Note that, for high aperture rates, the aperture shape is no longer circular due to the fact that the apertures should overlap the ligaments, which is not allowed in our calculations. Then the condition of identical aperture rate is not observed. This artifact leads to an artificial permeability plateau corresponding to the "without membrane" permeability. Apart from this artifact, FEM results show that relationship between permeability and mean aperture is almost unaffected by the porosity (i.e., the width of ligaments).

This power-law relationship is in agreement with a local interpretation based on the pressure drop of the fluid passing through the aperture. Indeed, Sampson [23] solves analytically the problem of the pressure drop ΔP occurring for an incompressible fluid flow passing through a circular hole of diameter d_o in a thin plate:

$$\frac{q}{\Delta P} = \frac{d_o^3}{24\mu}, \tag{3}$$

where q is the volume fluid flow rate passing through the hole.

This relation arises from the fact that, at low Reynolds number, the coefficient of fluid resistance $\zeta = 2\Delta P/(\rho V_o^2)$, is, in general, proportional to the inverse of Reynolds number ${\rm Re} = V_o d_o \rho/\mu$ [24], where V_o is the mean stream velocity in the narrowest section of the orifice ($V_o = 4q/\pi d_o^2$).

After Ref. [25], the pressure drop through a hole of circular shape is very close to the one obtained with a hole of squared

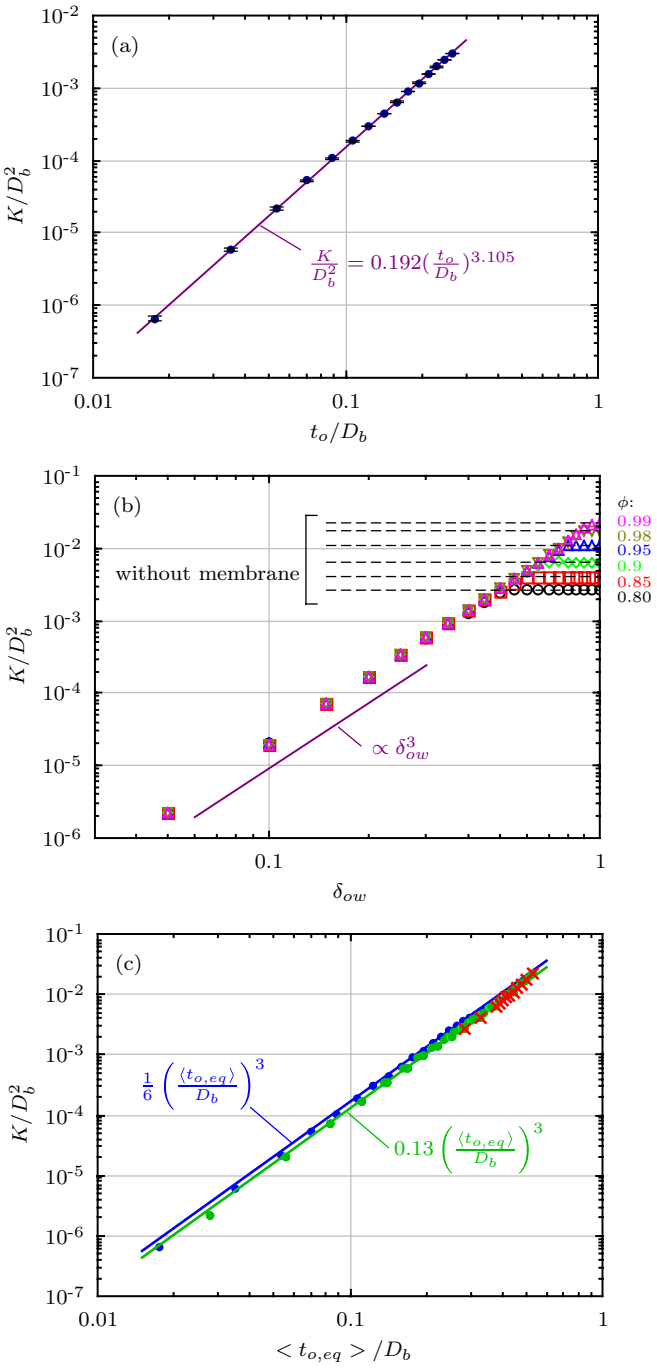

FIG. 4. (a) FEM results at identical aperture size with $\phi = 0.98$, (b) FEM results at identical aperture rate for various ϕ, (c) permeability as a function of the mean aperture: FEM results (blue dot for identical aperture, green dot for identical rate, red cross for "without membrane" foam with ϕ varying from 0.8 to 0.99), pore-network model with Sampson local permeabilities and $N_v = 14$ (blue line for identical aperture, green line for identical rate). Note that the mean aperture is calculated without including the four square windows, which are parallel to the macroscopic flow direction $\langle t_{o,\mathrm{eq}}\rangle/D_b = (2t_{o,\mathrm{sq}} + 8t_{o,\mathrm{hex}})/10D_b$.

shape having the same area. We can deduce that the Sampson formula can be extended to various shapes of aperture by considering an equivalent diameter $t_{o,eq}$ defined from the surface area of the aperture S_o: $t_{o,\mathrm{eq}} = 2(S_o/\pi)^{0.5}$. By using such a definition for the aperture size and calculating a window average of the aperture size, we can plot all FEM results on a same graph, even those for which aperture is not perfectly circular. Figure 4(c) shows that all data, including the ones obtained without a membrane, follow the same trend. Therefore, the pressure drop in foam is governed by a local mechanism which is not described by the usual Hagen-Poiseuille equation as is done in classical porous media [15,17,18,20].

To check the ability of a pore-network model to predict the permeability, pore-network calculations were performed using local permeabilities given by a Sampson equation:

$$k = t_0^3/24D_b. \tag{4}$$

Note that in such simple simulated configurations (i.e., identical aperture size t_0 or identical aperture rate δ_{ow}), the pore-network problem shown in the previous section can be solved analytically. Therefore, macroscopic permeability is given by $K = 2k_{sq} + 2k_{hex}$, leading to $\frac{K}{D_b^2} = \frac{1}{6}(\frac{t_0}{D_b})^3$ for identical aperture size and $\frac{K}{D_b^2} = \frac{1+3^{1.5}}{12}(\frac{5}{1+48^{0.5}}\frac{\langle t_{o,eq}\rangle}{D_b})^3 \approx 0.13(\frac{\langle t_{o,eq}\rangle}{D_b})^3$ for identical aperture rate. Figure 4(c) shows that pore-network calculations compare very well to FEM results. This good agreement supports both the interpretation of the permeability by using local permeabilities and the relevance of pore-network simulations.

B. Effect of closed windows: The bond percolation problem in foam

Figure 5 shows the permeabilities calculated with FEM simulations performed on large samples having random positions of closed windows and various open window fractions x_{ow}. For $x_{\mathrm{ow}} > 0.3$, permeability exhibits a quasi-affine dependence on the open window fraction x_{ow}. Below a critical concentration $x_{\mathrm{ow}} < 0.2$, the fluid flow vanishes.

To check their capacity to reproduce FEM results, pore-network simulations were performed by using two local

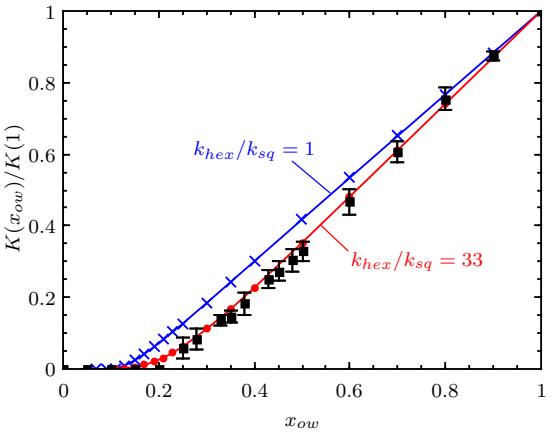

FIG. 5. Dimensionless permeability $K(x_{\mathrm{ow}})/K(1)$ as a function of open window fraction x_{ow} for FEM simulations (black square) and pore-network simulations (blue cross and red dot) on samples mixing two local permeabilities with various ratios k_{hex}/k_{sq} and having a Kelvin structure ($N_v = 14$). Error bars are calculated using (maximal value–minimal value)/2.

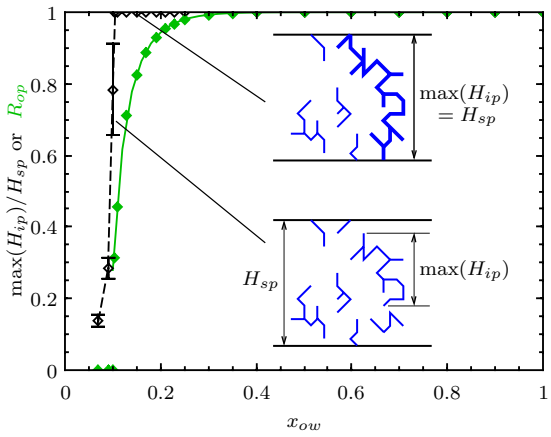

FIG. 6. Pore-network simulations: Height of the largest cluster of interconnected pores (black diamond) and fraction of open porosity (green diamond) as a function of the open window fraction x_{ow} for $N_v = 14$ and large samples $N_p \sim 10^6$. Green line corresponds to fraction of open porosity calculated by using Eq. (6a).

permeabilities, k_{hex} and k_{sq}, given by the Sampson equation and associated to squared and hexagonal windows as in Kelvin's structure ($N_v = 14$). For $\phi = 0.9$, the hexagonal-to-square aperture ratio in FEM simulations is close to 3.2. The ratio between local permeabilities is therefore close to $k_{hex}/k_{sq} = 33$ ($\approx 3.2^3$). As shown in Fig. 5 and considering the margin of error, pore-network simulations and FEM simulations lead to the same results. Moreover, pore-network simulations reveal that the slope of the affine part of the function $K(x_{ow})$ depends on the ratio between local permeabilities.

In reference to percolation theory [14], solid foams are subject to bond percolation for which bonds correspond to open walls. In such a percolation problem, pore-network simulations are helpful to calculate the heights of interconnected pores H_{ip}, the fraction of open porosity R_{op} (= number of pores within open pore space N_p'/total number of pores, N_p), and permeability [14,26]. In the case $N_v = 14$, the maximal height of interconnected pores is equal to the sample thickness H_{sp} for $x_{ow} > 0.1$, and percolation occurs (Fig. 6). This fraction corresponds to the percolation threshold x_p and is close to $1.5/N_v$ for all lattices studied as in Ref. [14]. Therefore, as the average number of open windows per pore is equal to $x_{ow}N_v$, at least 1.5 open windows per pore are required to allow fluid flow through porous foamy materials. With respect to permeability (Fig. 7), simulations performed with homogeneous local permeabilities show that the slope of the affine part of $K(x_{ow})$ depends on the number of neighbor pores N_v. The affine part of $K(x_{ow})$ intercepts the abscissa to a critical value given by $x^\star_{ow} = 2/N_v$. Figure 7(b) shows that the ratio $K(x_{ow})/K(1)$ in porous material having homogeneous local permeability is linearly dependent on a single parameter $(x_{ow} - x^\star_{ow})/(1 - x^\star_{ow})$ except for open window fractions close to the percolation threshold.

A deeper analysis of our results makes it possible to study in detail the structure of the open-pore space and the one of fluid flow passing through it. Figure 8(b) shows that the fraction of open windows within the open pore space, x'_{ow}, is larger than the global value x_{ow}. This additional amount of open

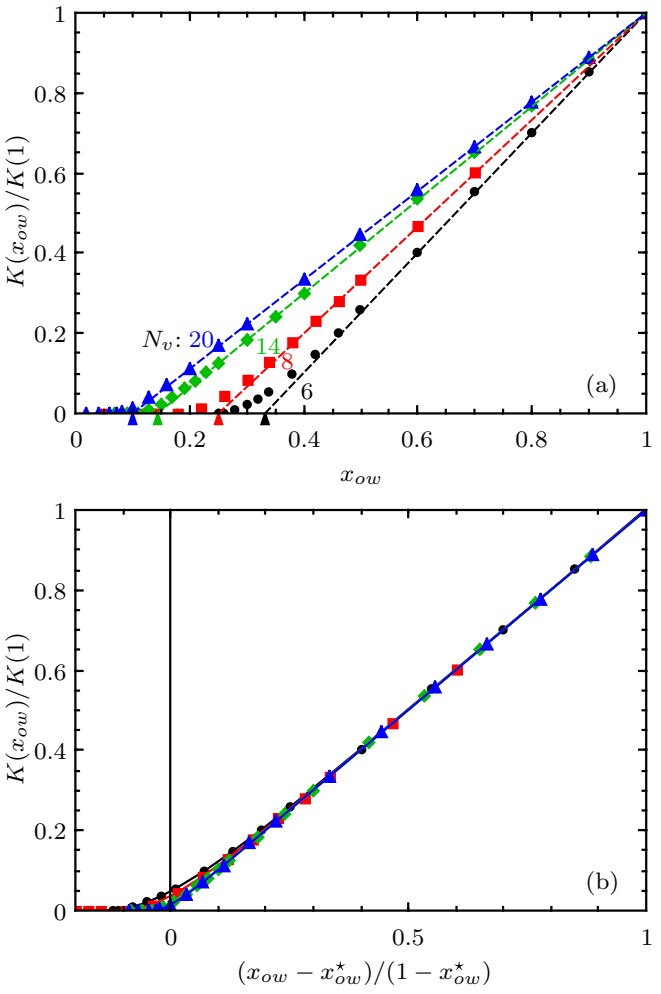

FIG. 7. Pore-network simulations: (a) dimensionless permeability $K(x_{ow})/K(1)$ as a function of open window fraction x_{ow} for various neighbor pores number N_v (arrows point to the abscissa $x_{ow} = x^\star_{ow} = 2/N_v$); (b) same data with another abscissa $(x_{ow} - x^\star_{ow})/(1 - x^\star_{ow})$.

windows within the open pore space can explain the behavior of permeability close to the percolation threshold. Indeed, by plotting the reduced fraction of open windows within the open pore space, $(x'_{ow} - x^\star_{ow})/(1 - x^\star_{ow})$, as a function of the open window fraction x_{ow} [Fig. 9(a)], we find curves which are very similar to the ones obtained for permeability as a function of x_{ow}. Moreover, from pore-network simulations, we can calculate the fraction of pores in which fluid flow occurs, $R_{op,flow}$ (= number of pores in which flow occurs/total number of pores). It appears that fluid flows occur only in a part of the open pore space; the other part of the open pore space is made of dead ends where no fluid flow occurs [Fig. 9(b)].

From a practical point of view, accurate formulas allowing us to estimate the fraction of open porosity R_{op}, the open window fraction within the open pore space x'_{ow}, and the percolation threshold x_p by measuring the open window fraction and the average number of neighbor pores could be useful. First, the threshold percolation x_p can be estimated by a formula given in Ref. [27]. Then, by considering the structure of closed pore clusters, it seems possible to calculate the

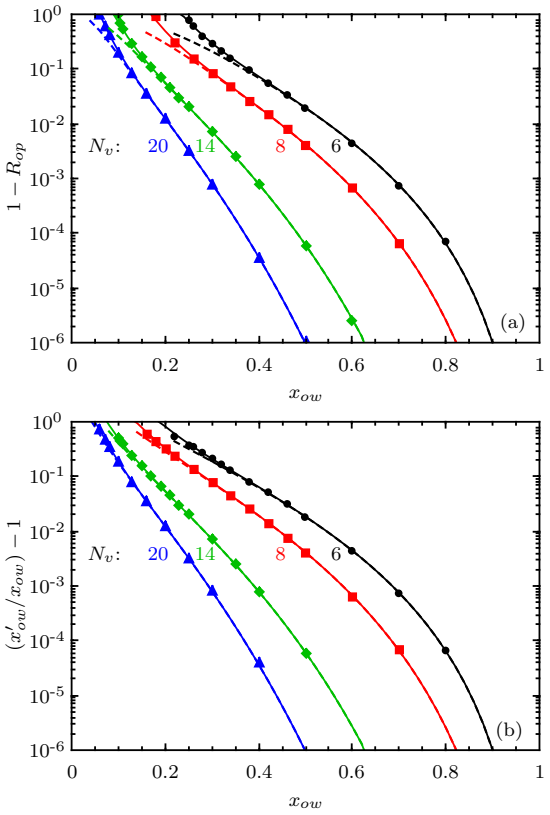

FIG. 8. Fraction of closed porosity, $1 - R_{op}$ (a) and excess fraction of open windows within the open pore space (b) as a function of the reduced fraction of open windows for various neighbor numbers N_v and large samples ($N_p \sim 10^6$). Dashed lines correspond to theoretical curves calculated by considering the first simplest closed clusters [Eqs. (5a) and (5b)]. Full lines correspond to curves calculated by using approximate formulas [Eqs. (6a) and (6b)].

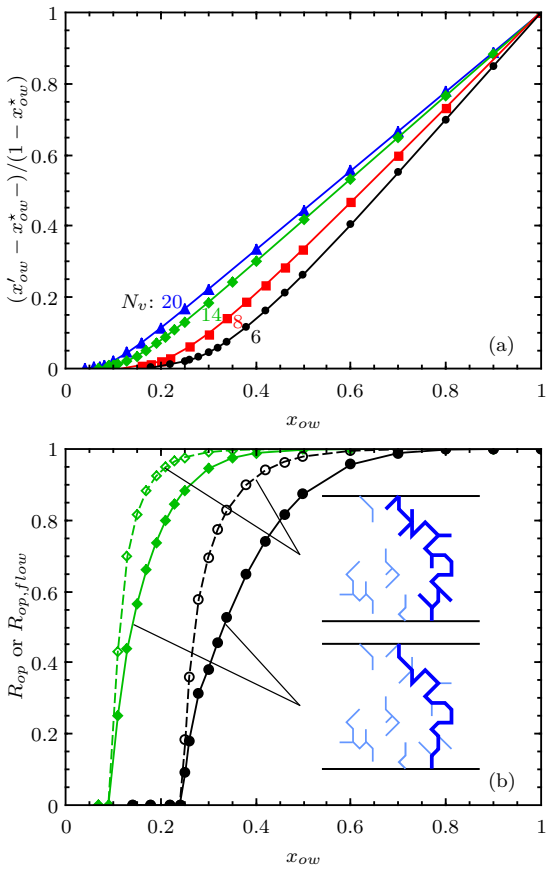

FIG. 9. Pore-network simulations: (a) $(x'_{\rm ow} - x^{\star}_{\rm ow})/(1 - x^{\star}_{\rm ow})$ as a function of open window fraction $x_{\rm ow}$ for various neighbor pores number N_v, (b) Open porosity fraction (dashed line) and open porosity fraction without dead ends (full line) as a function of the open window fraction $x_{\rm ow}$ for $N_v = 6$ (black) and $N_v = 14$ (green).

fraction of open porosity and the open window fraction within the open pore space. To begin, we calculate the fraction of pores P_k being within the first simplest closed clusters (Table I). For values of $x_{\rm ow}$ close to 1, those simplest closed clusters represent the main part of the closed pore space (i.e., pore space located outside open pore space). Then the fraction of open porosity $R_{op} = \frac{N'_p}{N_p}$ and the ratio $x'_{\rm ow}/x_{\rm ow} = (\frac{N'_{\rm ow}}{N'_p})/(\frac{N_{\rm ow}}{N_p})$ are given by

$$R_{op} \approx 1 - \sum_{k=0}^{3} P_k, \tag{5a}$$

$$\frac{x'_{\rm ow}}{x_{\rm ow}} \approx \frac{1}{1 - \sum_{k=0}^{3} P_k}\left(1 - \frac{2}{x_{\rm ow} N_v}\sum_{k=1}^{3}\frac{k}{k+1}P_k\right). \tag{5b}$$

Figure 8 shows that these approximated formulas are able to predict the fraction of open porosity and the ratio $x'_{\rm ow}/x_{\rm ow}$ except for open window fractions close to the percolation threshold where the complexity of the closed clusters structures increases drastically. To bridge the remaining gaps between theoretical calculations and numerical simulations, $x'_{\rm ow}$ and R_{op} can be approximated by the following equations, for $x_{\rm ow} > x_p$:

$$R_{op} \approx 1 - \sum_{k=0}^{3} P_k - \exp\left[-(3N_v + 12)\left(x_{\rm ow} - 1.88 N_v^{-1.2}\right)\right], \tag{6a}$$

$$\frac{x'_{\rm ow}}{x_{\rm ow}} \approx \frac{1}{1 - \sum_{k=0}^{3} P_k}\left(1 - \frac{2}{x_{\rm ow} N_v}\sum_{k=1}^{3}\frac{k}{k+1}P_k\right) + \exp\left[-(2.9N_v + 8.2)\left(x_{\rm ow} - 1.69 N_v^{-1.35}\right)\right], \tag{6b}$$

with $x_p = 0.7541[\frac{2}{3}(N_v - 1)]^{-0.9346}$ (from Ref. [27]).

Figures 6 and 8 show that these approximated formulas accurately predict $x'_{\rm ow}$ and R_{op} in the full range of $x_{\rm ow}$: $[x_p, 1]$.

C. Effective medium model for permeability

In this section, we present an effective medium model for permeability of pore-network built from the same theoretical framework as that of pore-network simulations. This model is based on a self-consistent calculation of the mean local permeability and a calculation of the macroscopic permeability. Details leading to Eqs. (7) and (8) are given in the Appendix.

TABLE I. Structures of simplest closed clusters having k open windows and $k+1$ pores, and fraction of pores P_k contained within such cluster (= total number of pores being in a closed cluster having k open windows and $k+1$ pores/total number of pores, N_p). In the "Closed cluster" drawing, open windows have a probability $x_{\rm ow}$, and closed windows (thin gray lines) have a probability $(1-x_{\rm ow})$.

k	Closed cluster	P_k
0		$(1-x_{\rm ow})^{N_v}$
1		$N_v x_{\rm ow}(1-x_{\rm ow})^{2N_v-2}$
2		$\frac{3}{2}N_v(N_v-1)x_{\rm ow}^2(1-x_{\rm ow})^{3N_v-4}$
3	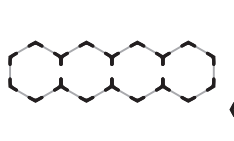	$\frac{1}{6}N_v(N_v-1)(13N_v-17)x_{\rm ow}^3(1-x_{\rm ow})^{4N_v-6}$

The mean local permeability $\bar{k}$ is calculated iteratively from [8,14]

$$\frac{1}{\bar{k}+n\bar{k}} = \sum_i \frac{x_i}{k_i+n\bar{k}} \tag{7}$$

with x_i the fraction of local permeability k_i and $n = \frac{N_v}{2} - 1$.

The macroscopic effective permeability is then deduced from the mean local permeability $\bar{k}$,

$$K = \sigma_w \bar{k}, \tag{8}$$

where the coefficient σ_w depends on the structure of the porous medium (Table II).

In a few simple cases, Eqs. (7) and (8) possess analytical solutions. This is the case for fully open-cell foam ($x_{\rm ow}=1$) described by a binary mixture of local permeabilities (see the Appendix). EM model is known to accurately predict the permeability of such a binary mixture of local permeabilities, but also to fail in its prediction for porous media having an open window fraction close to the percolation threshold [8,14]. To illustrate this point, consider the case of a porous medium having a mixture of closed windows and open windows characterized by an unique aperture parameter. The local permeability associated to the closed windows is equal to zero, and Eqs. (7) and (8) have an analytical solution:

$$\frac{K}{K_1} = \frac{x_1 - x_{\rm ow}^\star}{1-x_{\rm ow}^\star} \tag{9}$$

with $K_1 = \sigma_w k_1$.

As shown in Fig. 10, this solution "EM0" reproduces correctly the linear relationship between the permeability and the parameter $(x_{\rm ow}-x_{\rm ow}^\star)/(1-x_{\rm ow}^\star)$ except for an open window fraction close to the percolation threshold. In the case of foamy material where the number of neighbor pores is usually close to 14 (except for low porosity $\phi \approx 0.6$), the previous equation gives a very good approximation on a large range of open window fraction (i.e., for $x_{\rm ow} > 3/N_v \approx 0.2$). However, EM predictions can be improved if the open pore-space structure is explicitly considered. Indeed, since in the framework of the effective medium model, the mean local permeability is calculated by considering that the mean

TABLE II. Coefficients σ_w for used lattices and weakly disordered foam. Note that for SC, BCC, or Kelvin lattices, σ_w is isotropic.

Structure	SC	BCC	Kelvin	$N_v = 20$	Random foam
N_v	6	8	14	20	$2(n+1)$
σ_w	1	2	4	$\frac{14}{\sqrt{3}}$	$\approx\frac{n}{2}$

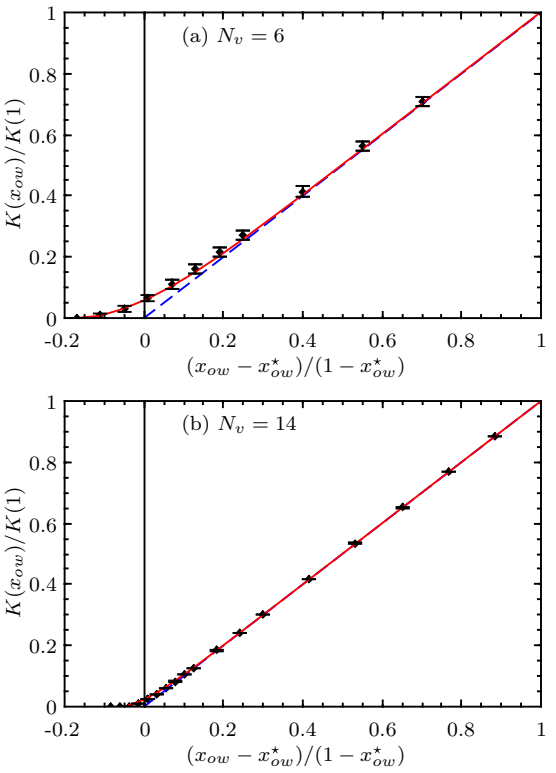

FIG. 10. Comparison between EM model and network simulations (black diamond) for various neighbor pore numbers. "EM0" (dashed blue line) is based on the global open window fraction [Eq. (9)], and "EM1" (red line) is based on the open window fraction within the open pore space [Eq. (10)].

fluid flow passes through the mean pore, the calculation of permeability should be performed on a half pore contained within the open pore space. Therefore, as shown in Fig. 10, by considering the structure of the open pore space in the calculation of permeability, via the percolating fraction of porosity R_{op} and the fraction of open windows within the open pore space x'_{ow} instead of the global open window fraction, the EM model predictions are significantly improved for open window fraction close to the percolation threshold. In this modified EM model "EM1," permeability is given by

$$\frac{K}{K_1} = \frac{x'_1 - x^{\star}_{\mathrm{ow}}}{1 - x^{\star}_{\mathrm{ow}}} R_{op}. \tag{10}$$

The fraction of open porosity R_{op} and the fraction of open windows within the open pore space can be estimated from the global open window fraction by using Eqs. (6a) and (6b).

For generalization purposes, one can write

$$\frac{1}{\overline{k'} + n\overline{k'}} = \sum_i \frac{x'_i}{k_i + n\overline{k'}}, \tag{11a}$$

$$K = R_{op}\sigma_w \overline{k'}, \tag{11b}$$

where x'_i is the fraction of windows within the open pore space having a local permeability equal to k_i. Note that the fraction of closed windows (for which $k_0 = 0$) within the open pore space, x'_0, is equal to $1 - \sum_{i\neq 0} x'_i$.

After Eq. (10), the physical meaning of the critical concentration $x^{\star}_{\mathrm{ow}} = 2/N_v$ is now more explicit: at least two open windows per pore located in the open pore space are required to start a sufficient interconnection of pores.

Other improvements of effective medium approximations based on real-space renormalization were proposed in the literature [8,28]. However, as the renormalization scheme depends on the lattice structure, a specific study for each lattice should be done.

IV. CONCLUSION

In order to study the effects of both the fraction of open windows and their aperture sizes on solid foam permeability, we performed different numerical simulations at different scales: FEM simulations computing the Stokes problem both at the pore scale and at the macroscale, and pore-network simulations of simplified flow performed on large lattices of interconnected pores. The FEM simulations at pore scale were useful to identify the pressure drop mechanism for fluid flow through solid foam and to define the local permeability associated with it. Thus, we show that the pressure drop inside fully open-cell foam can be explained by a mechanism acting at the scale of the membrane aperture and well described by Sampson's law [Eq. (4)]. The FEM simulations at macroscale with various fractions of open windows showed the ability of pore-network simulations to predict the permeability of percolating foamy medium. By using large samples, pore-network simulations results exhibit that percolation occurs when the fraction of open windows is close to $x_p = 1.5/N_v$ ($\approx$0.11 for foam having $N_v = 14$), and reveal that the fraction of open windows within the open pore space is a key parameter to interpret the particular behavior of permeability for fraction of open windows close to the percolation threshold x_p.

Finally, we developed a model of effective foam permeability allowing for foam permeability to be estimated by an analytical calculation [Eqs. (4), (6), and (11)]. In an alternative way to Sahimi et al. [28], the proposed approach modifies Kirkpatrick's model by introducing two parameters depending on the structure of the open pore space: the fraction of open porosity R_{op} and the fraction of open windows within the open pore space (x'_{ow}). However, Kirkpatrick's model with local permeabilities derived from the Sampson equation [i.e., Eqs. (4) and (9)] provides an excellent approximation for estimating permeability of foamy material having an open window fraction greater than 0.2.

By using an appropriate local permeability estimate, our approach to derive the effective permeability of porous materials could be extended to more complicated microstructures such as topologically disordered foams or materials exhibiting a hierarchical porosity.

ACKNOWLEDGMENT

This work was part of a project supported by ANR under Grants No. ANR-13-RMNP-0003-01 and No. ANR-13-RMNP-0003-03.

APPENDIX: EFFECTIVE MEDIUM THEORY

Here we detail the calculation of the mean local permeability. We consider a cross section of foam [Fig. 11(a)] and calculate the mean local permeability $\bar{k}$ of a foam containing different local permeabilities $\{k_i\}$. To represent a pore inside the cross section, we consider a half pore connected to $N_v/2$ effective pores such as $n = \frac{N_v}{2} - 1$ windows have a local permeability equal to the mean local permeability $\bar{k}$, and the last one located at the pth position has a local permeability equal to k_i [Fig. 11(b)]. Due to the heterogeneity induced by the local permeability k_i, the pressure inside the central pore $P_{i,p}$ is different from the mean pressure $\bar{P}$. Pressures inside

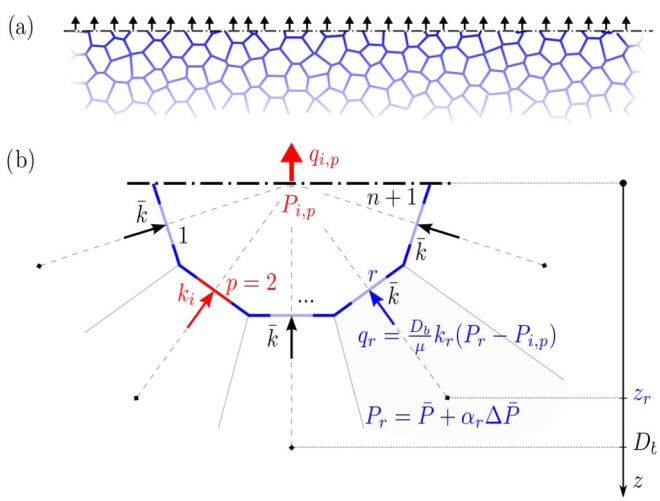

FIG. 11. (a) Cross section of foam; (b) geometry of a half pore representative of pores contained inside the foam cross section. Note that we have to consider $n+1$ configurations for the position p of the window associated with the local permeability k_i. Figure depicts the case $p = 2$.

neighbor effective pores are supposed equal to the effective pressure expected for each peculiar position of the neighbor pore: $\bar{P} + \alpha_r \Delta\bar{P}$ with $\alpha_r = z_r/D_b$. The total flow rate passing through the central half pore is equal to $q_{i,p} = \frac{D_b}{\mu}\sum_{r=1}^{n+1} q_r = \frac{D_b}{\mu}\sum_{r=1}^{n+1} k_r(\bar{P} + \alpha_r\Delta\bar{P} - P_{i,p})$, where $k_r = \bar{k}$ for $r \neq p$, and k_i for $r = p$.

The total flow rate can be written in a more useful way as

$$q_{i,p} = \frac{D_b}{\mu}\left[\sum_{r=1}^{n+1}\bar{k}(\bar{P} - P_{i,p} + \alpha_r\Delta\bar{P}) + (k_i - \bar{k})(\bar{P} - P_{i,p} + \alpha_p\Delta\bar{P})\right].$$

The effective flow rate $\bar{q}$ passing through the effective pore is obtained by considering $k_i = \bar{k}$ and $P_{i,p} = \bar{P}$ in the previous equation: $\bar{q} = \frac{D_b}{\mu}\sum_{r=1}^{n+1}\bar{k}\alpha_r\Delta\bar{P}$.

Therefore, the flow rate $q_{i,p}$ can be expressed in function of $\bar{q}$:

$$q_{i,p} = \bar{q} + \frac{D_b}{\mu}[(n+1)\bar{k}(\bar{P} - P_{i,p}) + (k_i - \bar{k})(\bar{P} - P_{i,p} + \alpha_p\Delta\bar{P})].$$

Thereafter, we suppose that the total flow rate passing through the central half pore $q_{i,p}$ is equal to the effective flow rate $\bar{q}$ leading to $0 = (n+1)\bar{k}(\bar{P} - P_{i,p}) + (k_i - \bar{k})(\bar{P} - P_{i,p} + \alpha_p\Delta\bar{P})$.

This hypothesis leads to the pressure inside the central pore:

$$P_{i,p} = \bar{P} + \frac{(k_i - \bar{k})}{n\bar{k} + k_i}\alpha_p\Delta\bar{P}.$$

Now, we may impose the self-consistency condition, requiring that the average $\langle P_{i,p}\rangle_{p,i} = \langle\langle P_{i,p}\rangle_p\rangle_i$ is equal to the effective pressure $\bar{P}$ leading to

$$\left\langle\frac{k_i - \bar{k}}{n\bar{k} + k_i}\right\rangle_i \langle\alpha_p\rangle_p\Delta\bar{P} = 0.$$

The previous equation can be rewritten in an alternative form:

$$\left\langle\frac{1}{n\bar{k} + k_i}\right\rangle_i = \frac{1}{(n+1)\bar{k}}.$$

To determine the macroscopic effective permeability, we have to calculate the macroscopic flow rate Q passing through the whole cross section A containing N_w windows having a local permeability equal to $\bar{k}$. Thus, assuming the effective gradient of pressure around the cross section $\frac{\Delta\bar{P}}{D_b}$ is equal to the mean pressure gradient $\frac{\Delta P_{sp}}{H}$, the macroscopic flow rate is given by

$$Q = \frac{D_b}{\mu}\left[\sum_{p=1}^{N_w}\alpha_p\right]\bar{k}\frac{\Delta P_{sp}}{H}D_b,$$

leading to the macroscopic effective permeability:

$$K = \sigma_w\bar{k},$$

where $\sigma_w = [\sum_{p=1}^{N_w}\alpha_p]\frac{D_b^2}{A}$

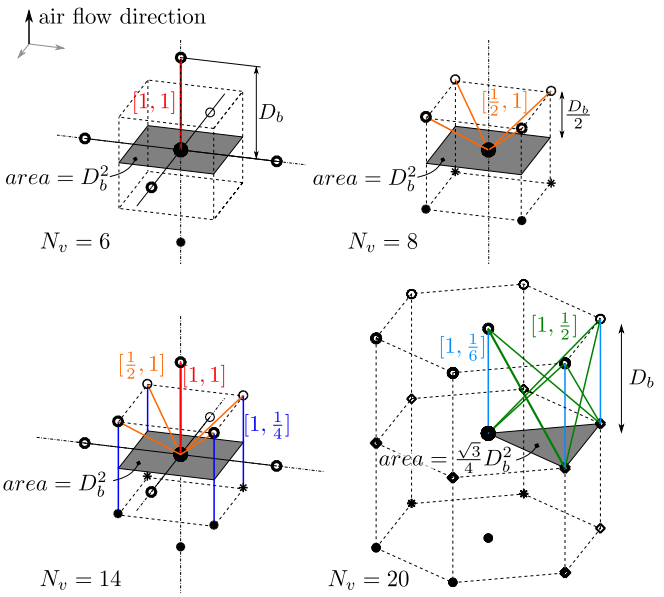

FIG. 12. For each lattice, bonds per unit cross section (gray area) considered for the calculation of σ_w. A couple (α_p, fraction of bonds p_b included within unit cross section) are associated to each bond. σ_w is calculated by $\sum\alpha_p p_b D_b^2/\text{area}$.

For each lattice, the calculation of σ_w is straightforward if we use the inclination of the cross section shown in Fig. 12. However, for SC, BCC, or Kelvin lattices, numerical calculations performed with various inclinations show that σ_w is isotropic. In the case of a weakly disordered foam (i.e., lowly polydisperse foam), we can use $\sigma_w = N_w\langle\alpha\rangle_p\frac{D_b^2}{A}$ and consider the continuous limit for the calculation of $\langle\alpha\rangle_p$ leading to $\langle\alpha\rangle_p = \frac{1}{2\pi}\int_0^{2\pi}\int_0^{\pi/2}\sin(\theta)\cos(\theta)\,d\theta\,d\varphi = \frac{1}{2}$. By considering the surface window density N_w/A of a Kelvin structure which is approximately equal to n/D_b^2, we find $\sigma_w \approx \frac{n}{2}$.

In the case of a binary mixture of local permeabilities (e.g., fully open foam), the mean local permeability $\bar{k}$ is given by $\frac{\bar{k}}{k_\infty} = \frac{1}{2}\{\alpha + [\alpha^2 + 4(1-\alpha)\frac{k_0}{k_\infty}]^{0.5}\}$, with

$$\alpha = 1 - \frac{k_1k_2}{nk_0k_\infty}$$
$$k_\infty = k_{Voigt} = x_1k_1 + x_2k_2$$
$$k_0 = k_{Reuss} = (\tfrac{x_1}{k_1} + \tfrac{x_2}{k_2})^{-1}.$$

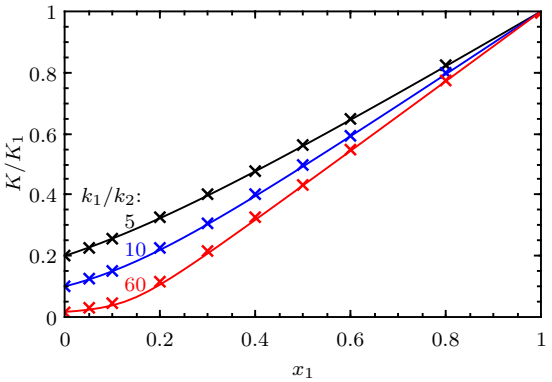

FIG. 13. Comparison of EM model predictions (full line) to network simulations (cross) with $N_v = 14$.

k_∞ and k_0 correspond respectively to the permeability of an infinitely interconnected network ($N_v \to \infty$) and the one of a poorly interconnected network ($N_v = 2$).

In such simple porous media, EM model accurately predicts the permeability calculated by pore-network simulations (Fig. 13).

[1] I. Cantat, S. Cohen-Addad, F. Elias, F. Graner, R. Höhler, O. Pitois, F. Rouyer, and A. Saint-Jalmes, *Foams: Structure and Dynamics* (Oxford University Press, Oxford, 2013).

[2] D. L. Johnson, J. Koplik, and R. Dashen, Theory of dynamic permeability and tortuosity in fluid-saturated porous media, J. Fluid Mech. **176**, 379 (1987).

[3] J. F. Allard and N. Atalla, *Propagation of Sound in Porous Media: Modelling Sound Absorbing Materials* (John Wiley & Sons, Chichester, 2009).

[4] O. Doutres, N. Atalla, and K. Dong, A semi-phenomenological model to predict the acoustic behavior of fully and partially reticulated polyurethane foams, J. Appl. Phys. **113**, 054901 (2013).

[5] M. T. Hoang and C. Perrot, Solid films and transports in cellular foams, J. Appl. Phys. **112**, 054911 (2012).

[6] P. Kumar and F. Topin, Predicting pressure drop in open-cell foams by adopting Forchheimer number, Int. J. Multiphas. Flow **94**, 123 (2017).

[7] C. Lusso and X. Chateau, Numerical Modeling of Disordered Foam in 3D: Effective Properties by Homogenization, *Proceedings of the sixth Biot Conference on Poromechanics, July 9-13, 2017* (Paris France, 2017), pp. 1347–1354.

[8] P. M. Adler, *Porous Media: Geometry and Transports* (Butterworth/Heinemann, Stoneham, MA, 1992).

[9] G. Mavko and A. Nur, The effect of a percolation threshold in the Kozeny-Carman relation, Geophysics **62**, 1480 (1997).

[10] H. L. Frisch, J. M. Hammersley, and D. J. A. Welsh, Monte Carlo estimates of percolation probabilities for various lattices, Phys. Rev. **126**, 949 (1962).

[11] H. K. Versteeg and W. Malalasekera, *An Introduction to Computational Fluids Dynamics: The Finite Volume Method* (Pearson Education, Pearson Education Limited, Harlow, UK, 2007).

[12] D. R. Duran, *Numerical Methods for Fluid Dynamics with Applications to Geophysics* (Springer-Verlag, New York, 2010).

[13] T. Krüger, H. Kusumaatmaja, A. Kuzmin, O. Shardt, G. Silva, and E. M. Viggen, *The Lattice Boltzmann Method—Principles and Practice* (Springer International Publishing, Switzerland, 2017).

[14] S. Kirkpatrick, Percolation and conduction, Rev. Mod. Phys. **45**, 574 (1973).

[15] H. J. Vogel, A numerical experiment on pore size, pore connectivity, water retention, permeability, and solute transport using network models, Eur. J. Soil Sci. **51**, 99 (2000).

[16] P. Van Marcke, B. Verleye, J. Carmeliet, D. Roose, and R. Swennen, An improved pore network model for the computation of the saturated permeability of porous rock, Transport Porous Med. **85**, 451 (2010).

[17] A. P. Jivkov, C. Hollis, F. Etiese, S. A. McDonald, and P. J. Withers, A novel architecture for pore network modeling with applications to permeability of porous media, J. Hydrol. **486**, 246 (2013).

[18] Q. Xiong, C. Joseph, K. Schmeide, and A. P. Jivkov, Measurement and modeling of reactive transport in geological barriers for nuclear waste containment, Phys. Chem. Chem. Phys. **17**, 30577 (2015).

[19] Q. Xiong, T. G. Baychev, and A. P. Jivkov, Review of pore network modeling of porous media: Experimental characterisations, network constructions and applications to reactive transport, J. Contam. Hydrol. **192**, 101 (2016).

[20] I. Fatt, The network model of porous media, I. Capillary pressure characteristics, Trans. AIME **207**, 144 (1956).

[21] C. Perrot, R. Panneton, and X. Olny, Periodic unit cell reconstruction of porous media: Application to open-cell aluminum foams, J. Appl. Phys. **101**, 113538 (2007).

[22] F. Hecht, New development in freefem++, J. Numer. Math. **20**, 251 (2012).

[23] R. A. Sampson, On Stokes's current function, Philos. T. Roy. Soc. A. **182**, 449 (1891).

[24] I. E. Idelchik, *Handbook of Hydraulic Resistance* (Begell House, New York, 1996).

[25] P. A. J. van Melick and B. J. Geurts, Flow through a cylindrical pipe with a periodic array of fractal orifices, Fluid Dyn. Res. **45**, 061405 (2013).

[26] B. Berkowitz and R.P. Ewing, Percolation theory and network modeling applications in soil physics, Surv. Geophys. **19**, 23 (1998).

[27] S. Galam and A. Mauger, Universal formulas for percolation thresholds, Phys. Rev. E **53**, 2177 (1996).

[28] M. Sahimi, B. D. Hughes, L. E. Scriven, and H. T. Davis, Real-space renormalization and effective-medium approximation to the percolation conduction problem, Phys. Rev. B **28**, 307 (1983).